Front. Mech. Eng. 2020, 15(2): 265–278
https://doi.org/10.1007/s11465-019-0571-9

RESEARCH ARTICLE

Ruichen WANG, Zhiwei WANG

Evaluation of power regeneration in primary suspension for a railway vehicle

Abstract To improve the fuel economy of rail vehicles, this study presents the feasibility of using power regenerating dampers (PRDs) in the primary suspension systems of railway vehicles and evaluates the potential and recoverable power that can be obtained. PRDs are configured as hydraulic electromagnetic-based railway primary vertical dampers and evaluated in parallel and series modes (with and without a viscous damper). Hydraulic configuration converts the linear behavior of the track into a unidirectional rotation of the generator, and the electromagnetic configuration provides a controllable damping force to the primary suspension system. In several case studies, generic railway vehicle primary suspension systems that are configured to include a PRD in the two configuration modes are modeled using computer simulations. The simulations are performed on measured tracks with typical irregularities for a generic UK passenger route. The performance of the modified vehicle is evaluated with respect to key performance indicators, including regenerated power, ride comfort, and running safety. Results indicate that PRDs can simultaneously replace conventional primary vertical dampers, regenerate power, and exhibit desirable dynamic performance. A peak power efficiency of 79.87% is theoretically obtained in series mode on a top-quality German Intercity Express track (Track 270) at a vehicle speed of 160 mile/h (~257 km/h).

Keywords railway vehicle, primary damper, power regeneration, ride comfort, running safety

Received April 17, 2019; accepted September 5, 2019

Ruichen WANG
Institute of Railway Research, University of Huddersfield, Huddersfield HD1 3DH, UK

Zhiwei WANG (✉)
State Key Laboratory of Traction Power, Southwest Jiaotong University, Chengdu 610031, China
E-mail: tpl_zw@163.com

1 Introduction

The possibility of using recoverable energy in vehicle suspension systems has elicited considerable attention in recent years. Various design concepts and arrangements of regenerative suspensions have been proposed and investigated for the recovery of energy from motion and vibration due to road/track disturbances. However, these studies have focused on energy conversion from kinetic energy to electricity in road transports [1–5].

Meanwhile, the potential for similar applications of power regenerating dampers (PRDs) to the rail sector remains to be explored. In a typical passenger rail vehicle, a considerable amount of motive energy is wasted by the resistance from track irregularity, the friction between moving parts, and thermal losses. The kinetic energy loss of primary and secondary dampers is one of the notable causes of energy loss in rail vehicles, with a total dissipated power between 3.5 and 3.8 kW per vehicle [6,7].

Zuo and Zhang [8] estimated potential energy regeneration in different possible applications, such as passenger cars, trucks, military vehicles, and rail cars, through theoretical modeling analysis. They demonstrated that 5–6 kW can be recovered from dampers on railway vehicles running on a typical American track [9]. Given that most studies on regenerative techniques for road vehicles have focused on potential and regenerated power, the current work aims to recover a considerable amount of power from a vertical primary damper in a rail vehicle.

Regenerative techniques for vehicle suspension systems can be classified into three major categories in accordance with their operating principles: mechanical, electromagnetic, and hydraulic regenerative suspensions [10,11]. Mechanical regenerative suspension typically uses hydraulic/pneumatic power to convert kinetic energy into potentially recoverable mechanical energy that can be stored for later use through control methods [12–17]. Electromagnetic regenerative suspension converts relative vibration isolation into linear or rotary motion using electric generators to produce recoverable electricity

[18–28]. Hydraulic regenerative suspension converts reciprocating linear motion into unidirectional rotary motion through a designed hydraulic circuit, and thus, produces electricity through a generator [29–33].

Motivated by previous studies, preliminary evaluation was simulated with four rail vehicle dampers (i.e., primary vertical, secondary lateral, secondary vertical, and secondary yaw dampers), with the PRD in parallel to each type of damper. This study aims to estimate power capability and adaptability to rail vehicle suspension systems. Therefore, a comparison of the power capability of different dampers in rail vehicles is presented in Table 1, along with power efficiency.

In the proposed PRD design, the power efficiency of the primary vertical damper reaches the highest efficiency of 3.75% when the rail car is running at 160 mile/h (~257 km/h) on a top-quality German Intercity Express (ICE) track (Track 270) with 10 Ω internal and external electrical loads. In addition, considering the damping characteristics of railway dampers (Table 2 and Fig. 1), PRD can replace a primary vertical damper to achieve higher regenerative output power. PRD allows adjustable damping, which is characterised by applying external load resistance, to alter the fluid flow of the hydraulic rectifier; PRD is similar to commercially used semi-active dampers, such as controllable magnetorheological and electrorheological dampers [34,35].

To improve power regenerating techniques in railway vehicles, a primary suspension system with efficient PRDs was designed and applied to a comprehensive rail vehicle model to characterise the dynamic response of the rail vehicle. Normally, the conventional viscous dampers transmit vibrations between the track and the vehicle carbody to ensure the capabilities of ensure ride comfort

Table 1 Comparisons among different railway dampers: Parallel configurations

Damper	Potential power/W	Regenerated power/W	Regenerated power efficiency/%
Primary vertical damper	39.07 (low)	1.47 (low)	3.75 (high)
Secondary lateral damper	4790.00 (high)	12.47 (high)	0.67 (low)
Secondary vertical damper	25.82 (very low)	0.32 (very low)	1.25 (moderate)
Secondary yaw damper	3700.00 (moderate)	3.03 (moderate)	0.08 (very low)

Table 2 Values of the parameters of a typical passenger rail vehicle [41]

Symbol	Definition	Value	Symbol	Definition	Value
m_{veh}	Total vehicle mass	3.3×10^4 kg	B_{wb}	Bogie wheelbase	2.6 m
m_{bd}	Carboy mass	2.508×10^4 kg	H_{bd}	Body height	1.57 m
m_{bg}	Total bogie frame mass	4.18×10^3 kg	H_{bg}	Bogie height	0.5 m
m_{ws}	Per wheelset mass	1.12×10^3 kg	W_r	Wheel radius	0.45 m
k_{sl}	Secondary lateral stiffness (per axle box)	1.672×10^6 N/m	H_{slbdh}	Secondary lateral damper body end height	0.53 m
c_{sl}	Secondary lateral damping (per damper×2)	2.507598×10^4 N·s/m	H_{slbgh}	Secondary lateral damper bogie end height	0.56 m
k_{sv}	Secondary vertical stiffness (per axle box)	1.3672×10^5 N/m	H_{svt}	Secondary vertical damper body end height	0.96 m
c_{sv}	Secondary vertical damping (per damper×4)	1.337386×10^4 N·s/m	H_{svb}	Secondary vertical damper bogie end height	0.895 m
k_{sy}	Secondary yaw stiffness (per axle box)	2.09×10^5 N/m	H_{syt}	Secondary yaw damper body end height	0.61 m
c_{sy}	Secondary yaw damping (per damper×4)	6.687×10^6 N·s/m	H_{sybgh}	Secondary yaw damper bogie end height	0.53 m
k_{pv}	Primary vertical stiffness (per axle box)	7.599×10^5 N/m	H_{pvt}	Primary vertical damper height (top)	0.81 m
c_{pv}	Primary vertical damping (per damper×8)	4179.33 N·s/m	H_{pvb}	Primary vertical damper height (bottom)	0.29 m
c_{ped} (Case 1)	Electrical damping (PRDs, c_{ped})	See Fig. 1(a)	L_{hl}	Half body length	12 m
c_{ped} (Case 2)	Electrical damping (PRDs, c_{ped})	See Fig. 1(b)	L_{hw}	Half body width	1.4 m

Note: Case 1: Total damping coefficient of the primary damper = $c_{pv} + c_{ped}$, $c_{pv} = 4.17933\times10^3$ N·s/m; Case 2: Total damping coefficient of the primary damper = c_{ped}, $c_{pv} = 0$ N·s/m.

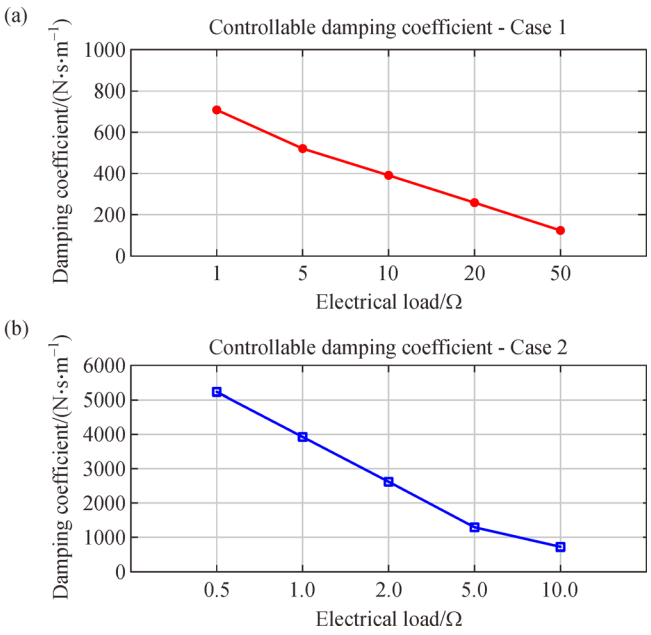

Fig. 1 Electrical damping coefficient with different electrical loads. (a) Case 1; (b) Case 2.

and running safety [8,36–38]. High levels of running safety and ride comfort can guarantee a constant increase in customer experience and safety requirements [36,39,40]. Therefore, these results have not only been used to investigate the capability of power regeneration and efficiency, but also to evaluate ride comfort and running safety performance by utilizing the design of PRDs.

The proposed PRD is configured to operate in parallel (Case 1) and series (Case 2) modes to elucidate the influences of damping characteristics and power capability on variable working conditions, such as running speeds, electrical loads, and measured tracks.

In this paper, references and previous studies are presented first. The preliminary evaluation of the power capability of railway dampers (primary vertical, secondary vertical, secondary lateral, and secondary yaw dampers) is also introduced. A comprehensive passenger vehicle model is presented in Section 2.1, and the irregularity of the measured tracks and the PRD system layout are described in Sections 2.2 and 2.3, respectively. Ride comfort and running safety in rail vehicles are discussed in Sections 2.4 and 2.5, respectively. Section 3 provides the impact factors of different operating conditions and components. Conclusions are summarised in Section 4.

2 System modeling

The dynamics of a passenger vehicle is extremely complex, with several significant nonlinearities and undefined variables, such as dynamic contact relations in the wheel–rail contact area, suspension systems, and track response. In general, most passenger rail vehicles exhibit a similar basic mode, as illustrated in Fig. 2, which shows a simplified side view of a half car. The carbody is supported

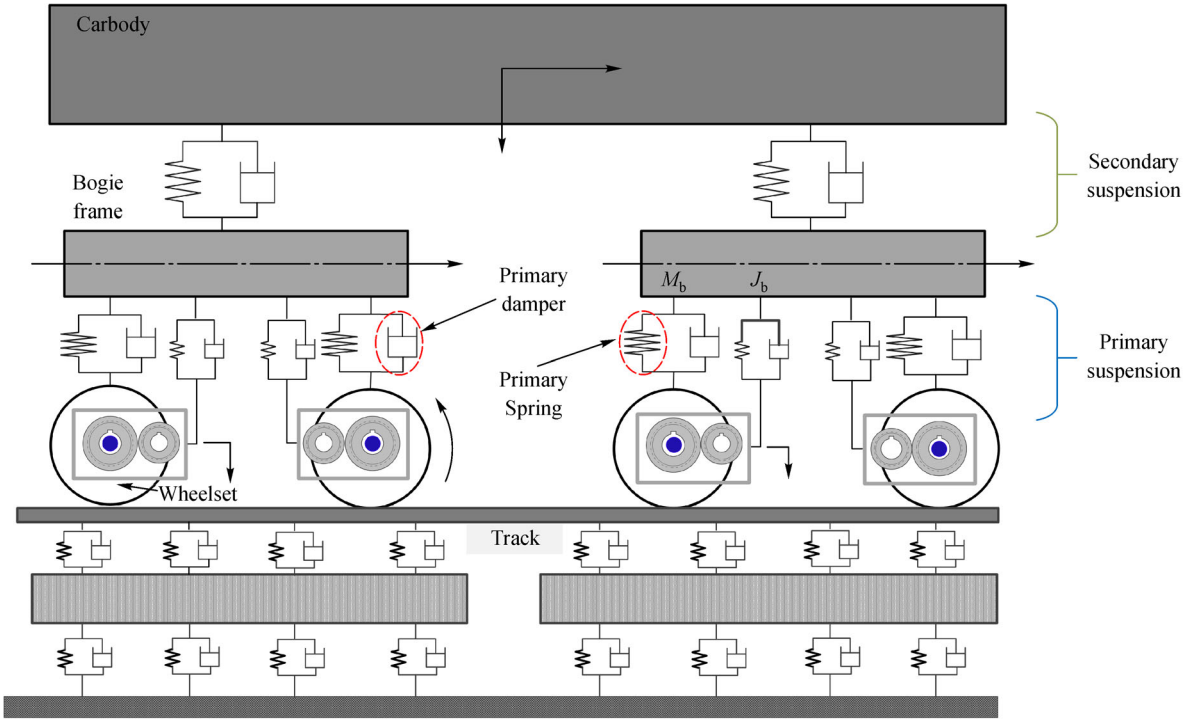

Fig. 2 Simplified side view of a rail vehicle.

by two bogies via the secondary suspension. In each bogie, the wheelsets are connected to the bogie by the primary suspension system (frequently consists of passive springs and dampers connected in parallel).

2.1 Rail vehicle model

In the modeling system, a PRD is installed in parallel with each primary vertical damper (Case 1) or replaces each primary vertical damper (Case 2) in a rail car to determine power and search for the optimal electrical damping (additional damping) in the vertical direction. The key parameters of a typical UK passenger vehicle are provided in Table 2 [41].

On the basis of the defined typical passenger vehicle model and track data, Fig. 3 shows the modeling procedure and performance evaluation, including track roughness, dynamic rail vehicle model, and rail vehicle response variables, in the time domain.

Vehicle modeling and objective function calculations are conducted in this domain under various driving speeds and track irregularities. The outputs include primary suspension vertical velocity, wheel–rail contact forces (i.e., lateral and vertical forces), weighted root-mean-square (RMS) accelerations of the body center, pivots 1 and 2 (in the longitudinal, lateral, and vertical directions), damping force, potential power, and recoverable power.

2.2 Track irregularity

The surface roughness of a track is the key source of track-induced vibration for a railway vehicle. Predefined tracks that use sinusoidal irregularity with a given frequency and amplitude and well-defined track inputs for the stochastic modeling of track geometry are insufficient for investigating the performance of a given suspension or damper system; thus, a more realistic measured track is used as input in this study, as shown in Table 3 [42].

2.3 Power regenerating damper

With the rapidly increasing demands for large energy in rail transport, recoverable energy in rail vehicle suspension systems must be developed for the energy conservation of future regenerative dampers in rail vehicles. Many designs are being developed for regenerative suspensions or dampers. Among them, the regenerative electrohydraulic damper exhibits the most potential due to its inherent design benefits of unidirectional flow with low inertia loss, reliable hydraulic transmission, and high regeneration efficiency [43–45]. A schematic design of the proposed PRD, which consists of a double acting hydraulic cylinder, a hydraulic rectifier (four check valve arrangement), a hydraulic motor, and a generator, is shown in Fig. 4.

Figures 4(a) and 4(b) show a simplified primary suspension system equipped with a PRD in parallel (Case 1) and series (Case 2) modes, respectively, which can be executed with a standard fluid viscous damper in parallel and series connections in the primary suspension system. Figures 4(a) and 4(b) show that m_1 and m_2 is the carbody and bogie mass. Viscous damping, electrical damping and equivalent damping of primary damper are defined as C_m, C_e and C_{eq}. C_1 is the damping of secondary damper. k_1 and k_2 are the spring stiffness of primary and secondary suspensions. R and r are external electrical load and internal resistance of the generator. L is the inductance of the generator. Notably, the PRD can provide desirable damping by adjusting the electrical load (R) to achieve

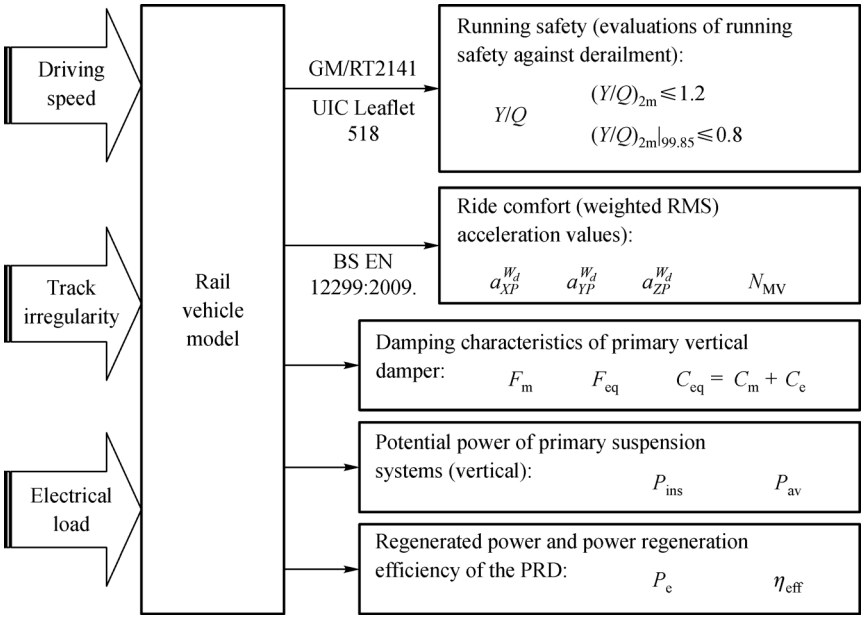

Fig. 3 Block diagram of the overall objective functions in a rail vehicle.

Table 3 General track data characteristics and descriptions [42]

Track	Line speed/(km·h^{-1})	Length/km	Standard deviation (lateral)/mm	Standard deviation (vertical)/mm	Description
110	110	5	3.04	5.12	A low-speed, 110 km/h (70 mile/h) piece of UK track, lower-quality cross-country track
160	160	5	2.46	2.77	A mainline UK track, 160 km/h (100 mile/h), typical of better-quality cross-country and lower-quality intercity routes
200	200	5	1.42	2.39	A good-quality piece of UK mainline track, 200 km/h (125 mile/h), typical of high-speed intercity tracks
225	225	5	1.36	2.00	Top-quality UK track, 225 km/h (140 mile/h), example of the best intercity track
270	270	4	1.04	1.81	Top-quality German ICE track, 270 km/h (170 mile/h)

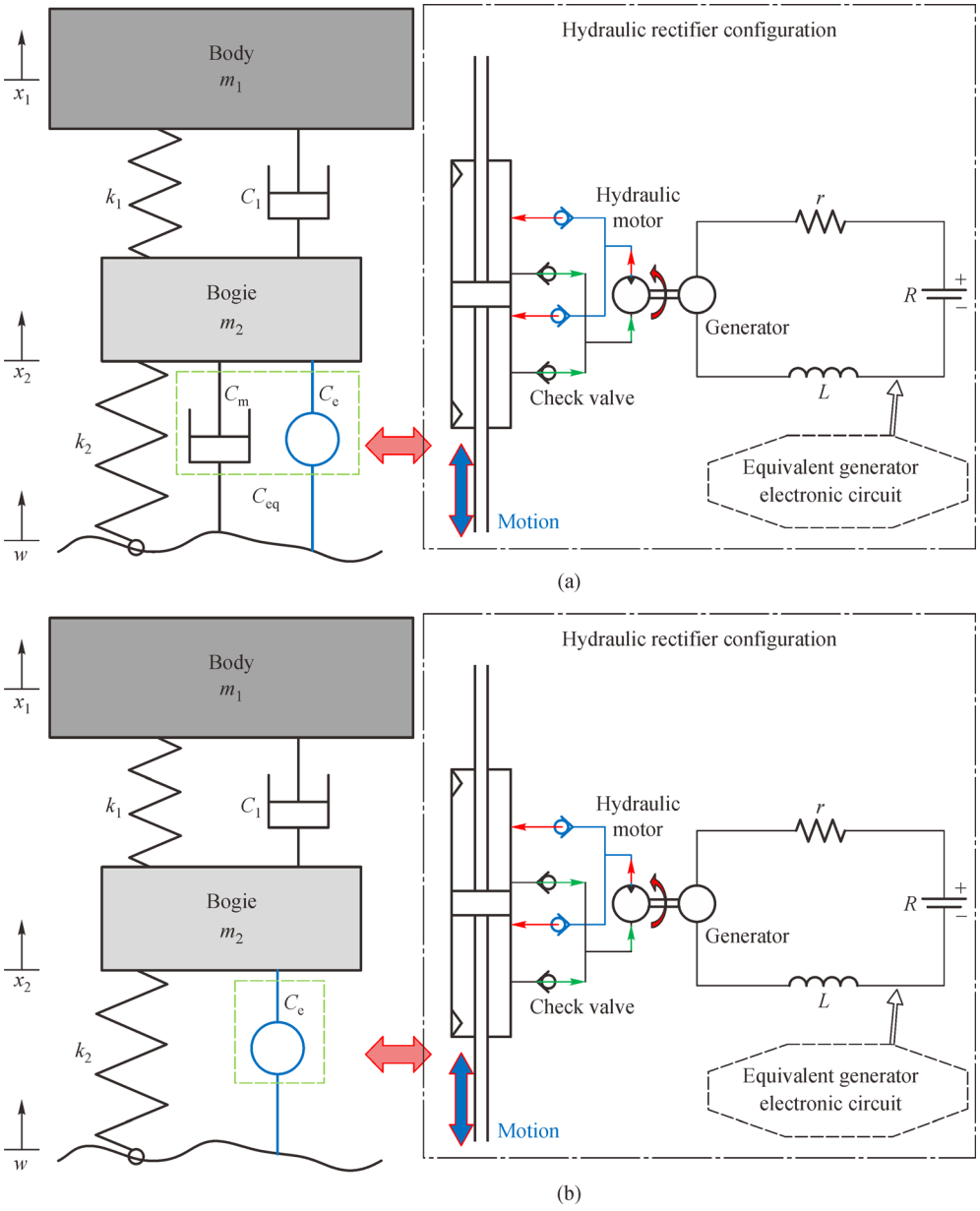

Fig. 4 Simplified diagram of the suspension systems and PRD. (a) Parallel: Case 1; (b) series: Case 2.

appropriate damping while recovering power for energy saving. The values of key parameters of the PRDs shows in Table 4.

The hydraulic cylinder is designed with four ports, which are distributed at both sides of the cylinder body. Four check valves are connected and act as a hydraulic rectifier. Through rectification, the hydraulic fluid passes through the hydraulic motor in one direction during bounce and rebound motions. The hydraulic motor is directly coupled to the generator and driven by pressuresed flow. The hydraulic motor converts the linear motion of the primary suspension system into rotary motion via fluid transfer, and then the succeeding rotation of the hydraulic motor drives the generator to produce electricity [33].

Using the PRD, energy from the track roughness-induced vibrations can be converted into recoverable energy, which can be stored in a battery/cell for further use, and an appropriate damping coefficient can be provided by adjusting electrical load, which can be further developed for semi-active or self-powered force control.

Several evaluation criteria for ride comfort, running safety, potential power, and regenerated power, which can be satisfied by the primary suspension system, are presented on the basis of a typical passenger rail vehicle model, the PRD, and measured track data. Evaluation is dependent on the potential power, recoverable power, power efficiency, wheel–rail contact forces, and acceleration of the carbody and bogies. This study aims to provide a design guideline for using a regenerative primary damper. The primary damper in a rail vehicle is not only for power generation, but also for achieving dynamic performance in terms of running safety and passenger comfort.

In the proposed system, the equivalent damping of the primary damper and the PRD can be written as

$$C_{\mathrm{eq}} = C_{\mathrm{m}} + C_{\mathrm{e}}, \tag{1}$$

where C_{eq} is the equivalent damping coefficient of the primary damper, C_{m} is the viscous damping coefficient, and C_{e} is the electric damping coefficient (controllable damping coefficient). The electric damping coefficient is [46]

$$C_{\mathrm{e}} = \left(\frac{2\pi A_{\mathrm{m}}}{D_{\mathrm{m}}}\right)^2 \frac{k_{\mathrm{T}} k_{\mathrm{V}}}{r+R} \frac{\eta_v}{\eta_{\mathrm{m}}}, \tag{2}$$

where A_{m} is the area of the hydraulic cylinder cross-sectional area, D_{m} is the displacement of the hydraulic motor, k_{T} is the torque constant coefficient, k_{V} is the electromotive voltage constant coefficient, r is the internal resistance of the generator, R is the external load, and η_{v} and η_{m} are the volumetric and mechanical efficiencies of the hydraulic motor, respectively. The hydraulic motor flow rate is expressed as follows:

$$Q_{\mathrm{m}} = A_{\mathrm{m}} v, \tag{3}$$

where v is the vertical velocity of the primary damper. The motor/generator shaft speed can be calculated as follows:

$$\omega_{\mathrm{m}} = \frac{2\pi Q_{\mathrm{m}} \eta_v}{D_{\mathrm{m}}}. \tag{4}$$

The generator used in the PRD should be mechanically simple for ease of functionality and operability. Therefore, an equivalent direct current (DC) permanent magnetic generator is modeled and embedded into the primary suspension system in this study. Electromotive force (EMF) is highly dependent on the generator's armature speed and field current.

EMF (E) and the instantaneous electrical current (I) are derived as follows:

$$E = k_{\mathrm{V}} \omega_{\mathrm{m}} \text{ and } I = \frac{E}{R+r}. \tag{5}$$

Regenerated power is the power recovered by the PRD for reuse and can be calculated as

$$P_{\mathrm{e}} = I^2 R. \tag{6}$$

The input power obtained from vibrational excitation is defined as the potential recoverable power and can be derived as follows:

$$P_{\mathrm{ins}} = c_{\mathrm{eq}} v^2. \tag{7}$$

The average potential power is

$$P_{\mathrm{av}} = \frac{1}{T}\int_0^T C_{\mathrm{eq}} v^2 \mathrm{d}t, \tag{8}$$

where T is the time end, and dt is the time interval. Table 3 provides the model-related component parameters of the PRD, such as the hydraulic rectifier and generator specifications.

From Eqs. (3)–(8), power regeneration efficiency is expressed as

$$\eta_{\mathrm{eff}} = \frac{P_{\mathrm{e}}}{P_{\mathrm{av}}} = \frac{2\pi T A_{\mathrm{m}} v \eta_{\mathrm{v}} \omega_{\mathrm{m}}}{D_{\mathrm{m}}(R+r)\int_0^T C_{\mathrm{eq}} v^2 \mathrm{d}t}. \tag{9}$$

Equation (2) represents the controllable damping coefficient of the PRD, and it shows that damping is dependent on electrical load. This equation indicates that the damping coefficient can be adjusted within a large

Table 4 Values of key parameters of the PRDs

$A_{\mathrm{m}}/\mathrm{m}^2$	$D_{\mathrm{m}}/(10^{-6}\ \mathrm{m}^3)$	$k_{\mathrm{T}}/(\mathrm{N\cdot m\cdot A^{-1}})$	$k_{\mathrm{V}}/(\mathrm{V\cdot rad^{-1}\cdot s})$	$\eta_{\mathrm{v}}/\%$	$\eta_{\mathrm{m}}/\%$	r/Ω	R (Case 1)/Ω	R (Case 2)/Ω
0.000127	8.2	0.925	0.925	92	95	10	1, 5, 10, 20, 50	0.5, 1, 2, 5, 10

range by controlling the external electrical load or the specific charge circuit. On this basis, the electrical damping coefficient (controllable damping coefficient) decreases with an increase in electrical load.

Figure 1 shows that electrical damping can act as additional/alternative damping when applied to the primary suspension system, allowing the adjustment of damping while recovering power for energy saving. In Fig. 1(a), a 1 Ω electrical load can provide a damping coefficient of approximately 710 N·s/m, which is approximately 1/6 of the viscous damping of the existing primary damper. Meanwhile, a larger electrical load of over 50 Ω provides less additional damping coefficient, which approaches toward zero. In addition, the damping coefficient of the PRD Case 2 altered with electrical loads is shown in Fig. 1(b). A 0.5 Ω electrical load is equivalent to a damping coefficient of approximately 5200 N·s/m, which is sufficient for a generic passenger rail vehicle. Therefore, the PRD can be adjusted within a large range by controlling external electrical loads. The PRD can also produce the required damping coefficient to replace the conventional primary vertical damper.

2.4 Ride comfort

The suspension system of modern passenger rail vehicles ensures good ride quality for passengers over different track irregularities. The suspension system acts as a key component for suppressing track-induced vibrations. Therefore, the system's dynamic performance significantly influences ride quality.

In accordance with the BS EN 12299:2009 standard for ride comfort-railway applications [47], the method involves filtering carbody accelerations time history (output in the longitudinal, lateral, and vertical directions), calculating the RMS at 5 s intervals, and determining the 95th percentile acceleration outputs over a time period of 5 min, are denoted as $a_{XP95}^{W_d}$, $a_{YP95}^{W_d}$ and $a_{ZP95}^{W_b}$. The 95th percentile accelerations are then entered into the following equation to determine the mean ride comfort index:

$$N_{\mathrm{MV}} = 6\sqrt{(a_{XP95}^{W_d})^2 + (a_{YP95}^{W_d})^2 + (a_{ZP95}^{W_b})^2}, \qquad (10)$$

where W_d is the weighted frequency value in accordance with x-axis (X-longitudinal direction) and y-axis (Y-lateral direction), W_b is the weighted frequency value in accordance with z-axis (Z-vertical direction) and P is the floor interface. On the basis of the particular interest of the ride comfort indices (N_{MV}), the standard for ride comfort indications is defined in Table 5 to provide a clear criterion.

Table 5 N_{MV} evaluation scales for ride comfort [36]

Scale for N_{MV}	Comfort index
$N_{\mathrm{MV}} < 1.5$	Very comfortable
$1.5 \leqslant N_{\mathrm{MV}} < 2.5$	Comfortable
$2.5 \leqslant N_{\mathrm{MV}} < 3.5$	Medium
$3.5 \leqslant N_{\mathrm{MV}} < 4.5$	Uncomfortable
$N_{\mathrm{MV}} \geqslant 4.5$	Very uncomfortable

2.5 Running safety

Running safety is determined by the wheel–rail contact forces (lateral and vertical), which are exchanged between the wheel and the rail, as shown in Fig. 5. One of the major risks of derailment is realised when a large lateral force and a low vertical force act between the wheel and the rail, allowing the wheel flange to climb up the rail gauge face rapidly and resulting in derailment. Therefore, the safety requirements for the wheel–rail contact performance of rail vehicles are considered key performance indicators.

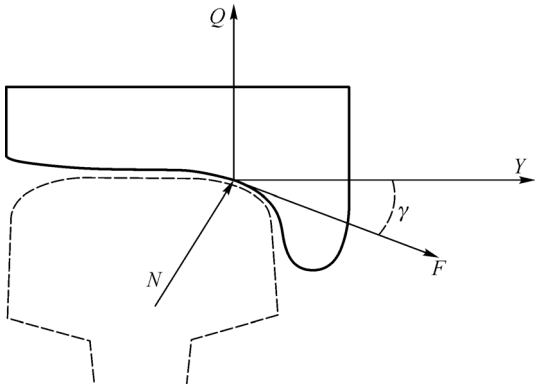

Fig. 5 Wheel–rail contact forces: Y (lateral force), Q (vertical force), N (normal force), and F (lateral rolling friction force).

The wheel–rail contact force ratio can be calculated in terms of lateral and vertical forces at various driving speeds and electrical loads. On the basis of the Nadal criterion [48] and GM/RT2141 [49], which must not exceed 1.2, this ratio can be expressed as follows:

$$\frac{Y}{Q} < \frac{\tan\alpha - \mu}{1 + \mu\tan\alpha}, \ \left(\frac{Y}{Q}\right)_{2\mathrm{m}} \leqslant 1.2, \qquad (11)$$

where μ is the friction coefficient at the contact point, and α is the maximum flange contact angle.

3 Analysis, results, and discussion

To evaluate ride comfort, running safety, potential power, and regenerated power, the rail vehicle primary suspension system developed in Section 2.3 was used under different vehicle running speeds, track cases, and electrical loads.

3.1 Ride comfort and running safety

To assess comparative ride performance under different

operating conditions, simulations were performed at a constant speed using approximately 30 km of the measured track geometry selected as a representative of the track seen by the modeled passenger rail vehicle. The simulation conditions can be summarised as follows:

Vehicle type: A generic 33 t passenger vehicle;

Wheel–rail contact: New P8 wheel, new 56E1 rail;

Track cases: ~30 km of measured track geometry;

Wheel–rail friction coefficient: 0.32;

Running speeds: 25, 50, 75, and 100 mile/h (with 1 Ω electrical load);

Electrical load (Case 1): 1, 5, 10, 20, and 50 Ω (100 mile/h running speed);

Electrical load (Case 2): 0.5, 1, 2, 5, and 10 Ω (100 mile/h running speed).

Accelerations were predicted on the vehicle body at the floor level above the leading and trailing bogie pivots and at the body center. Acceleration outputs were weighted in accordance with the lateral (W_d) and vertical (W_b) passenger comfort filters in Euro-Norm EN 12299:2009 [47]. The mean ride comfort of the body center, pivot 1, and pivot 2 were calculated under different running speeds and electrical loads, as presented in Tables 6 and 7.

Table 6 Ride comfort assessment (95th percentile weighted RMS acceleration (mean ride comfort)) under different vehicle speeds (load: 1 Ω)

Running speed/(mile·h^{-1})	Body center	Pivot 1	Pivot 2
Case 1			
25	0.6285	0.8265	0.9730
50	0.6924	1.3738	1.1074
75	0.8178	1.3696	1.4633
100	1.0422	1.7284	2.1450
Case 2			
25	0.6229	0.8158	0.9596
50	0.6790	1.3459	1.0770
75	0.8045	1.2948	1.4520
100	1.0401	1.7243	2.1318

Table 7 Ride comfort assessment (95th percentile weighted RMS acceleration (mean ride comfort)) under different vehicle speeds (viscous damper)

Running speed/(mile·h^{-1})	Body center	Pivot 1	Pivot 2
25	0.6285	0.8265	0.9730
50	0.6924	1.3738	1.1074
75	0.8178	1.3696	1.4633
100	1.0422	1.7284	2.1450

Mean ride comfort generally decreases with an increase in vehicle running speed at the body center, pivot 1, and pivot 2. In the worst case (100 mile/h) scenario, the mean ride comfort (N_{MV}) at pivot 2 reaches 1.68 but is still fairly comfortable for human vibration sensitivity. In addition, the ride performance of Case 1 is not dependent on the electrical load in the electric circuit of primary suspensions but is proportional to the increase of the electrical load in Case 2 at 100 mile/h. For comparison, the RMS accelerations of the original primary vertical damper are also analysed, and the results are presented in Tables 6 and 7. Evidently, the damping coefficients of the Cases 1–3 are applied using the following values: 4889, 3903, and 4179 N·s/m, respectively, on the basis of the values provided in Fig. 1. However, mean ride comfort is affected by the value of the equivalent damping coefficient, which can be altered by the electrical load in Cases 1 and 2. This phenomenon indicates that the less controllable damping coefficient in Case 2 can provide slightly improved ride comfort, particularly at a low electrical load. This phenomenon is also confirmed in Table 8.

Table 8 Ride comfort assessment (95th percentile weighted RMS acceleration (mean ride comfort)) under different electrical loads (speed: 100 mile/h)

Load resistance/Ω	Body center	Pivot 1	Pivot 2
Case 1			
1.0	1.0422	1.7284	2.1450
5.0	1.0422	1.7284	2.1450
10.0	1.0422	1.7284	2.1450
20.0	1.0422	1.7284	2.1450
50.0	1.0422	1.7284	2.1450
Case 2			
0.5	1.0401	1.7243	2.1318
1.0	1.0442	1.7367	2.1484
2.0	1.0507	1.7580	2.1702
5.0	1.0597	1.8010	2.2202
10.0	1.0668	1.8705	2.2781

Subsequently, simulations were conducted to examine the resistance of the proposed vehicle model to low-speed flange climbing derailment in accordance with the requirements of GM/RT2141 [49]. The following conditions were considered:

Wheel–rail friction coefficient: 0.32;

Running speed: 2 m/s (trundle);

Track cases: See Table 9.

Table 10 shows the ratio of the lateral force to the vertical force (Y/Q) for the leading wheelset outer wheel using different curve radii at 1 Ω. In all the cases, the predicted Y/Q remains below the Nadal limit of 1.2 and the 99.85 percentile limit of 0.8. The results of the maximum Y/Q slightly differ between Cases 1 and 2. Therefore, the results of the weighted RMS acceleration and Y/Q indicate that the applied PRD slightly influences ride comfort and

Table 9 Low-speed flange climbing track cases

Radius/m	Cant/mm	Gauge widening/mm	Transition length/m	Distance from the start of the runoff transition to the center of dip/m
90	25	19	7.5	0.000 (top), 7.500 (bottom)
150	100	13	30.0	6.000 (top), 16.883 (bottom)
200	150	6	45.0	6.000 (top), 16.883 (bottom)

Table 10 *Y*/*Q* low-speed flange climbing case under 1 Ω electrical load

Radius (transition*)/m	*Y*/*Q*		
	Case 1	Case 2	Case 3 (viscous damper)
90 (bottom)	0.714	0.714	0.714
90 (top)	0.699	0.699	0.683
150 (bottom)	0.605	0.605	0.605
150 (top)	0.760	0.760	0.761
200 (bottom)	0.726	0.723	0.715
200 (top)	0.676	0.675	0.676

Note: *Distance from the start of runoff transition to the center of dip.

running safety, but ride comfort and running safety are highly reliant on vehicle running speed, track irregularity, and track design.

3.2 Effect of running speed

Track input is the key impact of rail vehicle excitation, but the detailed relationship between track differences/running speeds and power capability has not been discussed in previous research. In accordance with the PRD and rail vehicle models, the force–velocity loops and power outputs at various speeds and tracks are obtained as shown in Figs. 6 and 7.

First, vehicle running speeds are modeled as the first influencing factor on power capability and damping characteristic. With the damping recalculation in Section 2.3, the equivalent damping coefficient of the primary damper is presented in Fig. 8, and the predicted results show the trend of the damping coefficient and damping force, which deteriorate with an increase in vehicle speed, and damping force highly depends on the surface geometry of the track. The potential power and increase with vehicle running speeds ranging from 25 to 125 mile/h at 25 mile/h intervals are clearly presented. However, vehicle running speed is the key factor of power regeneration in the proposed primary suspension system, and higher running speeds can provide higher flow rates of the hydraulic motor, accelerating the rotating speed of the DC generator, and finally, producing a larger damping force and higher power outputs. Therefore, running speed and track case are considered for the design and practical use of a PRD.

The damping forces between the series and parallel cases at different running speeds are shown in Figs. 6(a) and 6(c). These results indicate that damping characteristics have similar force–velocity loops at low running speeds (25 to 100 mile/h). At 125 mile/h, in accordance with the impact of a bump stop on the conventional primary vertical damper, the equivalent damping force (viscous and controllable damping forces) in the parallel case (Case 1) tends to be stable when the peak value exceeds 2100 N. In the series case (Case 2), the designed PRD replaces the conventional damper to provide a controllable damping force, and the peak damping force decreases with an increase in external electrical load. This phenomenon indicates that the series configuration is beneficial for providing a wide range of controllable damping forces by adjusting electrical load. It also demonstrates that PRD provides high construability for a self-powered and semi-active primary suspension.

Figure 7 illustrates that the average potential power and regenerated power are predicted at different measured tracks with vehicle running speed increasing from 25 to 125 mile/h with a 1 Ω electrical load in both cases. The power values increase slightly with vehicle speed. The faster the running speed, the more excitation events are produced, providing more potential power and regenerated power. However, power regeneration efficiency exhibits no evident increases. It is approximately 1.2% in the two cases.

At a running speed of 100 mile/h, high potential powers of 73.17 and 59.33 W can be obtained in Cases 1 and 2, respectively, when a rail vehicle runs on typical Track 160. This situation clearly shows that the regenerated power in primary suspension systems exhibits considerable potential to recharge the electronic equipment of a vehicle or achieve regenerative capability. A peak power of 26.06 W can be regenerated in Case 2 when the vehicle travels at 125 mile/h on a mainline UK track (Track 160). In accordance with the configuration of Case 1 (parallel), most of the potential power is dissipated in the form of heat by the conventional damper and the PRD to attenuate the vibrations produced by track-related excitation, and only a

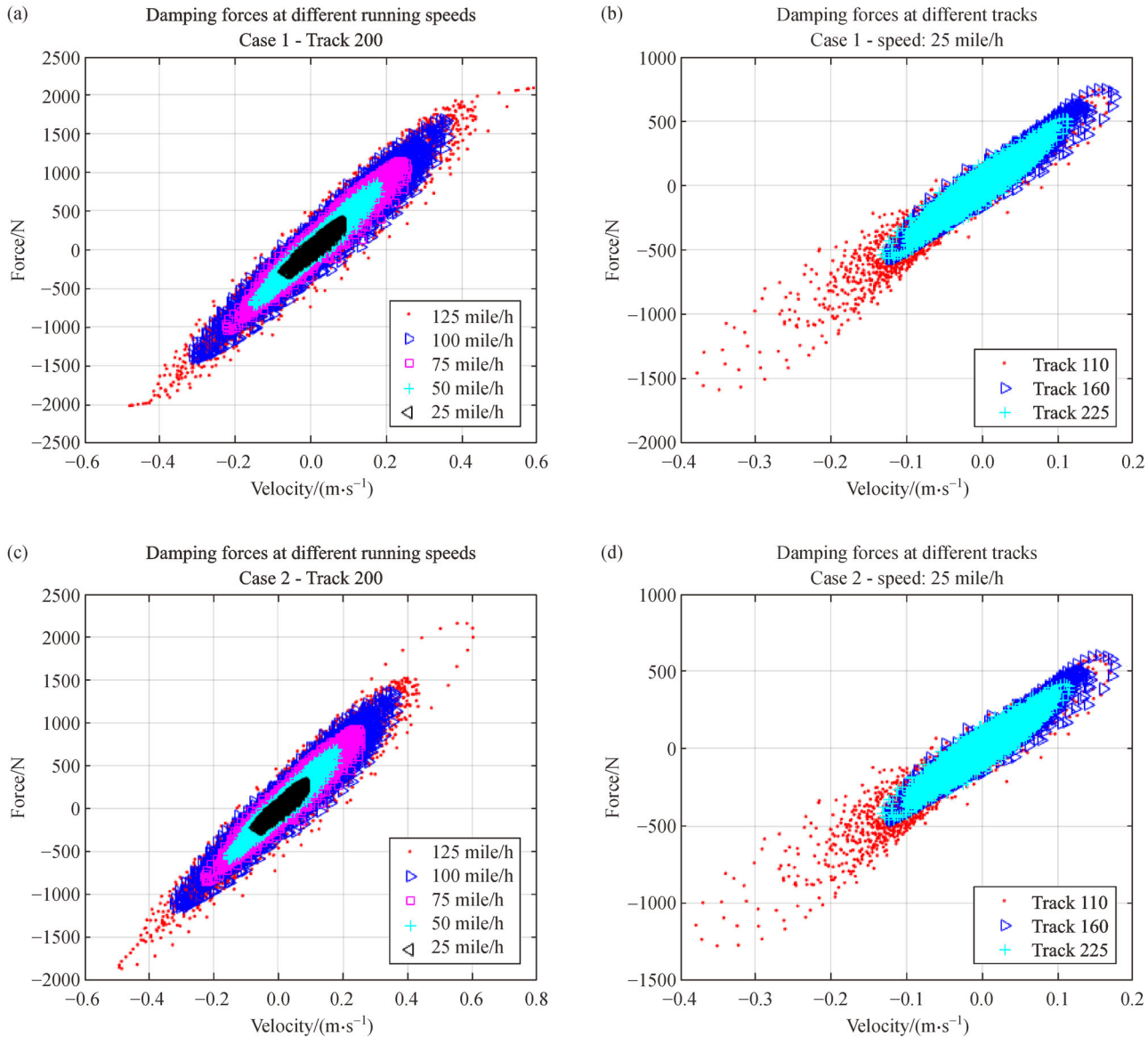

Fig. 6 Force-velocity loops. (a) Case 1 with Track 200 at different running speeds; (b) Case 1 with 25 mile/h speed at different tracks; (c) Case 2 with Track 200 at different running speeds; (d) Case 2 with 25 mile/h speed at different tracks.

small amount of power can be regenerated by the PRD. By contrast, in Case 2 (series), track-related excitation directly acts on the PRD to maximise its regenerative capability while providing the required consistent damping force for the suspension system.

3.3 Effect of electrical load

The following analysis explores the characteristics of potential power, regenerated power, and power efficiency under various electrical loads. In Fig. 8(a), an increase in electrical load exerts no significant effect on the potential power of the primary damper in Case 1. However, potential power decreases with the value of electrical load growth in Fig. 8(c).

Considering the increase in the controllable damping coefficient of the series configuration (Case 2: Without viscous damper), a considerable amount of regenerated power can be produced, as shown in Fig. 8(d), which is beneficial for improving the regenerative efficiency of power on PRD. Figures 8(b) and 8(d) clearly show that the regenerated power of Case 1 is significantly smaller that of Case 2 because a large amount of power is dissipated by the hydraulic system of the conventional damper. In addition, the regenerative efficiency of the PRD in Case 2 increases sharply with an increase in electrical load, whereas the regenerative efficiency of the PRD in Case 1 remains at a relatively low level, i.e., between 1% and 4%.

Figures 8(b) and 8(d) show that the maximum regenerated power is achieved under an electrical load of

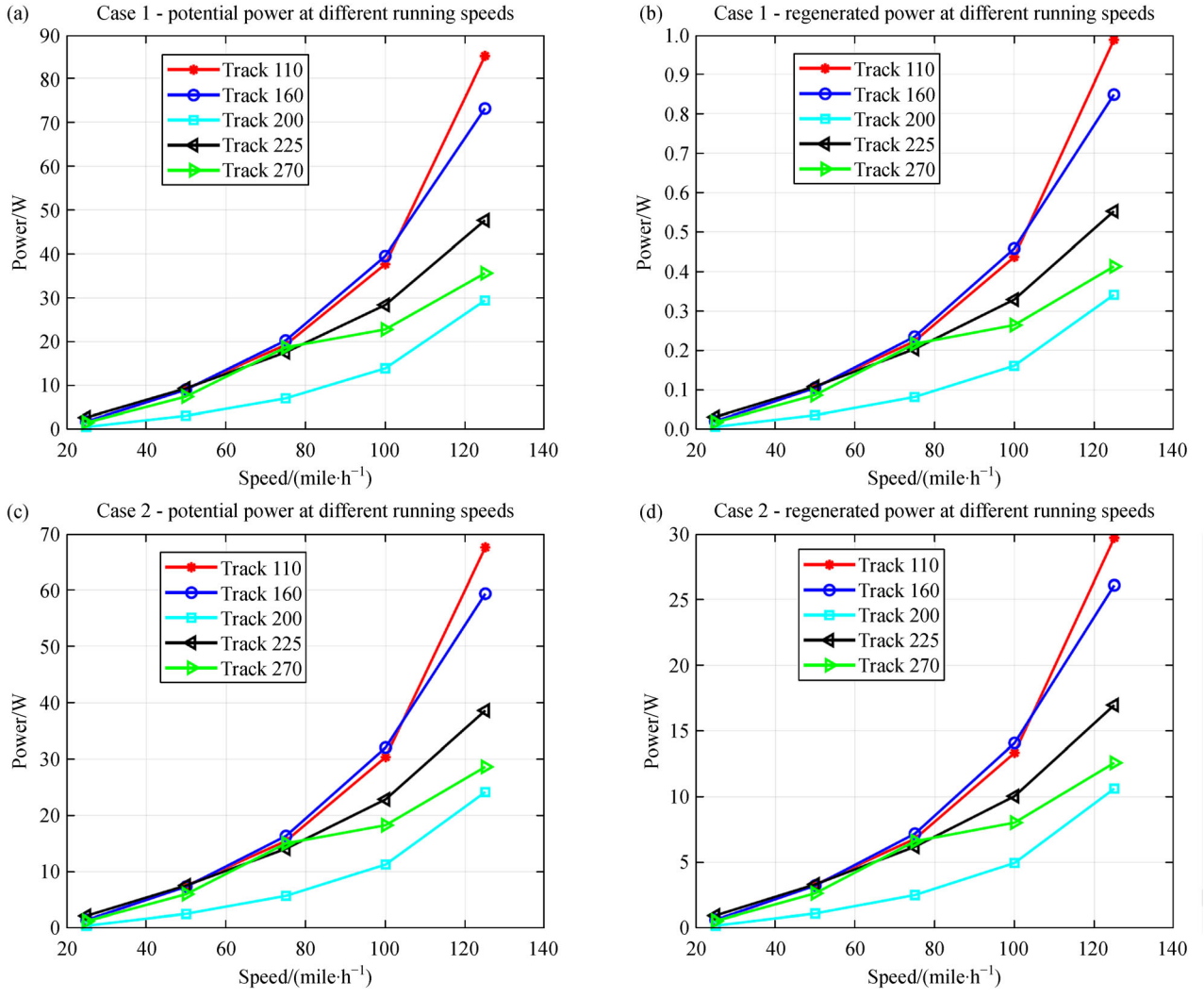

Fig. 7 (a) Case 1 potential power, (b) Case 1 regenerated power, (c) Case 2 potential power, and (d) Case 2 regenerated power at different running speeds.

1 Ω, and the maximum efficiency of 3.75% in Case 1 (Fig. 8(e)) is identical to the internal load resistance of the generator. This result indicates that the optimal power regeneration with maximum regenerating efficiency can be reached through impedance matching. In Case 2, power efficiency increases with the degradation of the damping coefficient (the growth of the external electrical load). As shown in Fig. 8(f), the peaks of power can be regenerated using the load resistance of 1 Ω under each running condition (track speed), but a maximum efficiency of 79.87% is obtained under an electrical load of 10 Ω (providing the minimum damping coefficient for the primary suspension system). This phenomenon occurs in response to a predefined top-quality German ICE track with a vehicle speed of 160 mile/h. Thus, the series configuration can effectively improve the capability of power regeneration while providing a suitable damping characteristic for the primary suspension system.

4 Conclusions

Power regeneration from railway vehicles that operate on irregular tracks and result in track-induced vibrations is an attractive field of vehicle dynamics. This study aims to capture and harvest energy lost due to track-induced vibrations from the primary suspension system based on more realistic measured tracks. A PRD was developed using two electrohydraulic configurations with and without a viscous damper (parallel and series). A detailed model of a typical UK passage vehicle with PRDs was developed to evaluate the potential power and regenerated power of the rail vehicle primary suspensions. Moreover, the influences of such a system on ride quality and running safety were investigated. For the proposed PRD, average power and efficiency were analysed under different vehicle running speeds, track qualities, and electrical loads. Regenerated power can be reused to satisfy the required power for

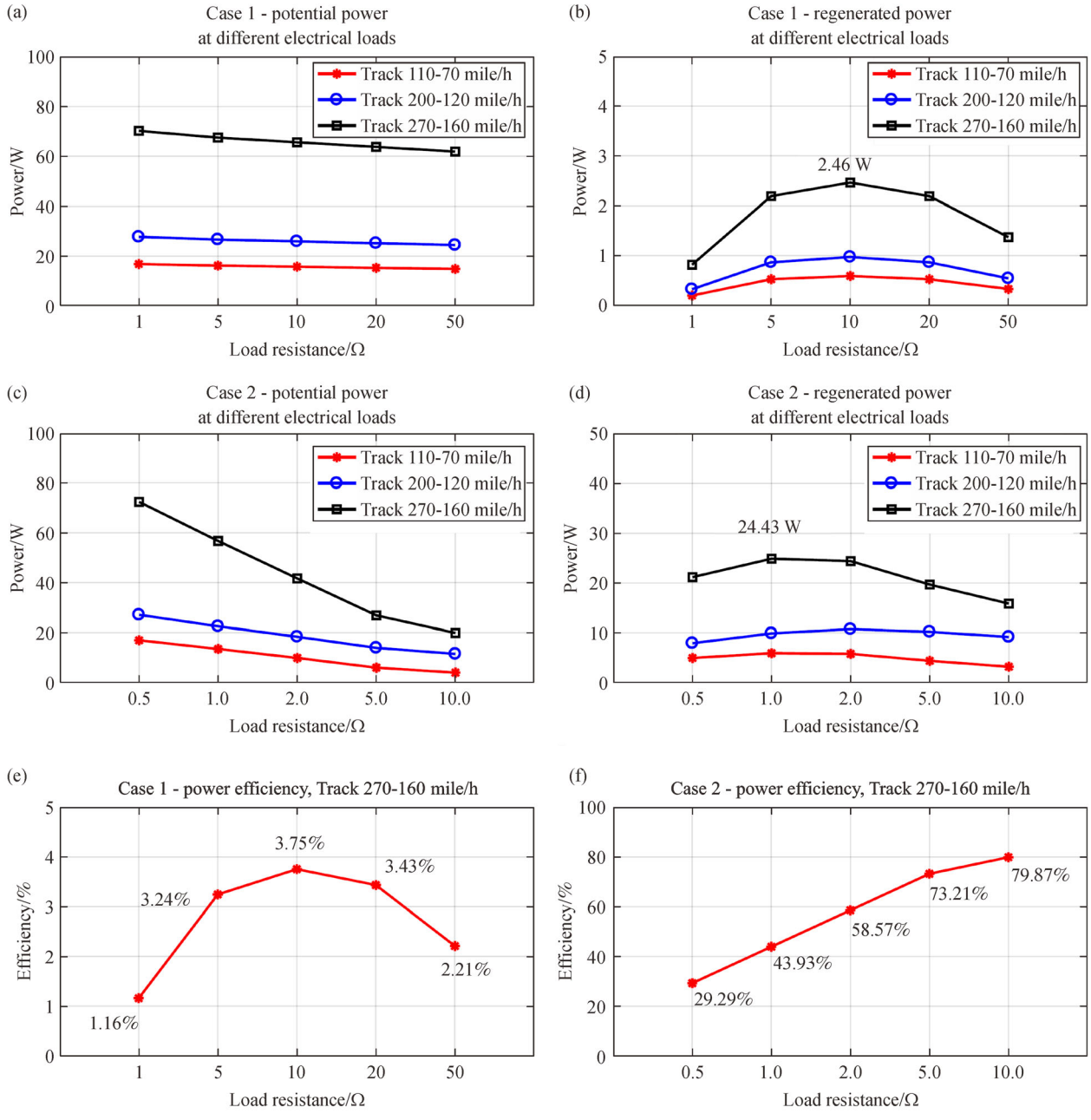

Fig. 8 (a) Case 1 potential power, (b) Case 1 regenerated power, (c) Case 2 potential power, (d) Case 2 regenerated power, (e) Case 1 power efficiency, and (f) Case 2 power efficiency at different electrical loads.

vehicle semi-active suspension or suspension electronic components.

The findings show the following:

1) The overall primary suspension system using the PRD in parallel and series connections delivered similar ride comfort and running safety as the conventional primary suspension system.

2) The increment of the external electrical load and running speed exerted no significant effect on the ride comfort and running safety of a rail vehicle.

3) The equivalent damping coefficient highly depends on electrical load, and the results show that better track quality can produce fewer excitation events, providing reduced peak damping force.

4) Using the measured track data as inputs, a potential power output of approximately 2–85 W is available for a single primary damper of a typical passenger rail vehicle at 125 mile/h on a poor-quality low-speed track, and the increase in vehicle speed will be a key factor of the positive action of power regeneration.

5) In accordance with the PRD design, the maximum efficiency (3.75%) of Case 1 at 10 Ω is identical to the internal resistance of the generator. In Case 2, the increase in the external electrical load is beneficial for power efficiency, which reaches 79.87% at 10 Ω. However, maximum power (24.43 W) can be regenerated at 1 Ω (which is identical to the internal resistance).

In summary, the series configuration can effectively improve the capability of power regeneration while providing a suitable damping characteristic for the primary suspension system. This design of the PRD can also be regarded as a semi-active regenerative damper by controlling electrical load to meet the requirements of different suspension systems. Therefore, the PRD can potentially replace the conventional primary damper.

Acknowledgements The authors are grateful for the financial support provided by the Sichuan Science and Technology Program (Grant No. 2019JDRC0081).

References

1. Yu F, Cao M, Zheng X. Research on the feasibility of vehicle active suspension with energy regeneration. Journal of Vibration and Shock, 2005, 24: 27–30 (in Chinese)
2. Karnopp D. Power requirements for vehicle suspension systems. Vehicle System Dynamics, 1992, 21(1): 65–71
3. Yu C, Wang W, Wang Q. Analysis of energy-saving potential of energy regenerative suspension system on hybrid vehicle. Journal of Jilin University (Engineering and Technology Edition), 2009, 39(4): 841–845 (in Chinese)
4. Liang J, Shao C. Research on an energy-regenerative active suspension for vehicles. Vehicle & Power Technology, 2010, (1): 55–58 (in Chinese)
5. Mossberg J, Anderson Z, Tucker C, et al. Recovering Energy from Shock Absorber Motion on Heavy Duty Commercial Vehicles. SAE Technical Paper 2012-01-0814, 2012
6. Matamoros-Sanchez A Z. The use of novel mechanical devices for enhancing the performance of railway vehicles. Dissertation for the Doctoral Degree. Loughborough: Loughborough University, 2013
7. Zheng P, Wang R, Gao J, et al. Parameter optimization of power regeneration on the hydraulic electric regenerative shock absorber system. Shock and Vibration, 2019, 2019: 5727849
8. Zuo L, Zhang P S. Energy harvesting, ride comfort, and road handling of regenerative vehicle suspensions. Journal of Vibration and Acoustics, 2013, 135(1): 011002
9. Zyga L. Energy-harvesting shock absorber that increases fuel efficiency wins R&D 100 award. Available at Science X website on July 14, 2011
10. Zhang J, Peng Z, Zhang L, et al. A review on energy-regenerative suspension systems for vehicles. In: Proceedings of the World Congress on Engineering. London, 2013, 1889–1892
11. Zheng P, Wang R, Gao J. A comprehensive review on regenerative shock absorber systems. Journal of Vibration Engineering & Technologies, 2020, 8(1): 225–246
12. Wendal G R, Stecklein G. A Regenerative Active Suspension System. SAE Technical Paper 910659, 1991
13. Fodor M G, Redfield R C. The variable linear transmission for regenerative damping in vehicle suspension control. In: Proceedings of American Control Conference. Chicago: IEEE, 1992, 26–30
14. Jolly M R, Margolis D L. Regenerative systems for vibration control. Journal of Vibration and Acoustics, 1997, 119(2): 208–215
15. Aoyoma Y, Kawabate K, Hsegawa S, et al. Development of the Full Active Suspension by Nissan. SAE Technical Paper 901747, 1990
16. Norisugu T. Energy saving of a pneumatic system (2). Energy regenerative control of a pneumatic drive system. Hydraulics & Pneumatics, 1999, 38(4): 1–4
17. Stansbury J. US Patent, 9270131. 2016-02-23
18. Karnopp D. Permanent magnet linear motors used as variable mechanical dampers for vehicle suspensions. Vehicle System Dynamics, 1989, 18(4): 187–200
19. Ryba D. Semi-active damping with an electromagnetic force generator. Vehicle System Dynamics, 1993, 22(2): 79–95
20. Gupta A, Mulcahy T M, Hull J R. Electromagnetic shock absorbers. In: Proceedings of the 21st International Modal Analysis Conference. Kissimmee, 2003, 181
21. Zuo L, Scully B, Shestani J, et al. Design and characterization of an electromagnetic energy harvester for vehicle suspensions. Smart Materials and Structures, 2010, 19(4): 045003
22. Okada Y, Yonemura J, Shibata M. Regenerative control of moving mass type vibration damper. In: Proceedings of the 4th International Conference on Motion and Vibration Control. Zurich, 1998, 85–90
23. Suda Y, Nakadai S, Nakano K. Study on the self-powered active vibration control. In: Proceedings of the 4th International Conference on Motion and Vibration Control. Zurich, 1998
24. Cao M, Liu W, Yu F. Development on electromotor actuator for active suspension of vehicle. Chinese Journal of Mechanical Engineering, 2008, 44(11): 224–228
25. Zheng X, Yu F. Study on the potential benefits of an energy-regenerative active suspension for vehicles. SAE Transactions, 2005, 114: 242–245
26. Li Z, Zuo L, Luhrs G, et al. Electromagnetic energy-harvesting shock absorbers: Design, modelling, and road tests. IEEE Transactions on Vehicular Technology, 2013, 62(3): 1065–1074
27. Hayes R J, Beno J H, Weeks D A. Design and Testing of an Active Suspension System for a 2-1/2 Ton Military Truck. SAE Technical Papers 2005-01-1715. 2005
28. Beno J H, Worthington M T, Mock J R. Suspension Trade Studies for Hybrid Electric Combat Vehicles. SAE Technical Paper 2005-01-0929, 2005
29. Zhang Y, Zhang X, Zhan M, et al. Study on a novel hydraulic pumping regenerative suspension for vehicles. Journal of the Franklin Institute, 2015, 352(2): 485–499
30. Fang Z, Guo X, Xu L, et al. Experimental study of damping and energy regeneration characteristics of a hydraulic electromagnetic shock absorber. Advances in Mechanical Engineering, 2013, 5: 943528
31. Li C, Tse P W. Fabrication and testing of an energy-harvesting hydraulic damper. Smart Materials and Structures, 2013, 22(6): 065024
32. Li C, Zhu R, Liang M, et al. Integration of shock absorption and

energy harvesting using a hydraulic rectifier. Journal of Sound and Vibration, 2014, 333(17): 3904–3916

33. Wang R, Gu F, Cattley R, et al. Modelling, testing and analysis of a regenerative hydraulic shock absorber system. Energies, 2016, 9(5): 386
34. Sharma S K, Saini U, Kumar A. Semi-active control to reduce lateral vibration of passenger rail vehicle using disturbance rejection and continuous state damper controllers. Journal of Vibration Engineering & Technologies, 2019, 7(2): 117–129
35. Sharma S K, Kumar A. Disturbance rejection and force-tracking controller of nonlinear lateral vibrations in passenger rail vehicle using magnetorheological fluid damper. Journal of Intelligent Material Systems and Structures, 2018, 29(2): 279–297
36. Sharma S K, Kumar A. Ride comfort of a higher speed rail vehicle using a magnetorheological suspension system. Proceedings of the IMechE, 2018, 232(1): 32–48
37. Sharma S K, Kumar A. Impact of longitudinal train dynamics on train operations: A simulation-based study. Journal of Vibration Engineering & Technologies, 2018, 6(3): 197–203
38. Sharma S K, Kumar A. Impact of electric locomotive traction of the passenger vehicle Ride quality in longitudinal train dynamics in the context of Indian railways. Mechanics & Industry, 2017, 18(2): 222
39. Sharma S K. Multibody analysis of longitudinal train dynamics on the passenger ride performance due to brake application. Proceedings of the IMechE, 2019, 233(2): 266–279
40. World Health Organization. Global status report on road safety: Time for action. Available at World Health Organization website on June 25, 2009
41. Serco. VTISM Version 2.6.6 User Guide, 2014
42. VAMPIRE Dynamics. Vehicle Dynamics Version 6.5. Resonate. Available at VAMPIRE website on July 1, 2016
43. Wang R. Modelling, testing and analysis of a regenerative hydraulic shock absorber system. Dissertation for the Doctoral Degree. Huddersfield: University of Huddersfield, 2016
44. Wang R, Chen Z, Xu H, et al. Modelling and validation of a regenerative shock absorber system. In: Proceedings of the 20th International Conference on Automation and Computing (ICAC'14). Cranfield: IEEE, 2014, 32–37
45. Wang R, Crosbee D, Iwnicki S, et al. Power regeneration in the primary suspension of a railway vehicle. In: Proceedings of the First International Conference on Rail Transportation. Chengdu, 2017
46. Xu L, Guo X X, Liu J. Evaluation of energy-regenerative suspension structure based on fuzzy comprehensive judgment (FCJ). Advanced Materials Research, 2010, 139–141: 2636–2642
47. BS EN 12299. Railway applications. Ride comfort for passengers. Measurement and evaluation. 2009
48. Nadal J. Theory of Locomotive Stability, Part II: Yaw Motion. Annals of Mines, 1896, 232–255
49. RSSB. Railway Group Standard GM/RT2141: Resistance of railway vehicles to derailment and roll-over. 2009